Smart Structures and Systems, *Vol. 15, No. 3 (2015) 769-785*
DOI: http://dx.doi.org/10.12989/sss.2015.15.3.769

Performance monitoring of timber structures in underground construction using wireless SmartPlank

Xiaomin Xu[*1], Kenichi Soga[1], Sarfraz Nawaz[1], Neil Moss[2], Keith Bowers[2] and Mohammed Gajia[2]

[1]Department of Engineering, University of Cambridge, Cambridge, UK
[2]Transport for London, London, UK

(Received November 8, 2014, Revised January 20, 2015, Accepted February 21, 2015)

Abstract. Although timber structures have been extensively used in underground temporary supporting system, their actual performance is poorly understood, resulting in potentially conservative and over-engineered design. In this paper, a novel wireless sensor technology, SmartPlank, is introduced to monitor the field performance of timber structures during underground construction. It consists of a wooden beam equipped with a streamlined wireless sensor node, two thin foil strain gauges and two temperature sensors, which enables to measure the strain and temperature at two sides of the beam, and to transmit this information in real-time over an IPv6 (6LowPan) multi-hop wireless mesh network and Internet. Four SmartPlanks were deployed at the London Underground's Tottenham Court Road (TCR) station redevelopment site during the Stair 14 excavation, together with seven relay nodes and a gateway. The monitoring started from August 2013, and will last for one and a half years until the Central Line possession in 2015. This paper reports both the short-term and long-term performances of the monitored timber structures. The grouting effect on the short-term performance of timber structures is highlighted; the grout injection process creates a large downward pressure on the top surface of the SmartPlank. The short and long term earth pressures applied to the monitored structures are estimated from the measured strains, and the estimated values are compared to the design loads.

Keywords: wireless sensor network; timber structure; underground construction; grouting; earth pressure

1. Introduction

Integrated in modern excavation and supporting systems, timber remains an important ground supporting material since the inception of underground construction (Mark and Barczak 2000, Mackenzie 2014). In early tunnels, timber was used for the initial or temporary support, followed by a permanent lining of brick or stone masonry. At present, timber support of temporary work continues to be an effective system for ground support, due to its availability, flexibility and ease of installation. It is preferred over steel mainly as: (1) it has a lower density (~420 kg/m^3) for transportation; and (2) it offers more flexibility, as it can be easily sawn, manipulated and put in the form of a support on site to suit specific local requirements whenever arise. As a construction material, timber requires none of the special equipments necessary for the placement of concrete or

∗Corresponding author, Ph.D., E-mail: xx787@cam.ac.uk

http://www.techno-press.org/?journal=sss&subpage=8 ISSN: 1738-1584 (Print), 1738-1991 (Online)

steel support, which demands a carefully dimensioned and engineered excavation for their installation. Nevertheless the principal disadvantage of timber as a support method is higher material cost and labor cost associated with its labor-intensive installation. This not only poses health and safety risks to workers, but also increases the cost and construction time. Therefore, in any situation if used, it should be able to bear the load safely and its consumption should be minimized /optimized to economize on its material and construction costs.

Despite its extensive usage in underground construction, the actual performance of the timber supporting temporary works has not been thoroughly understood, resulting in often conservative and over-engineered design. Until recently, temporary timbering support is solely relying on the experience of the contractor and analogies from the mining industry. An estimation of loads on underground temporary structures is principally based on the classical recommendations by Terzaghi (1946) and some historic practices. The former is probably only adequate for relatively shallow tunnels in favorable ground conditions (Kavvadas 2003), while the latter is considered by the industry to lead to over-engineered structures. For instance, the short-term and long-term horseheads in the London Underground are designed to carry at least 25% and 40% of the soil overburden, respectively (Mackenzie 2014). In order to cater for the different loading conditions in the field and in the laboratory, the strength of timber in the underground environment is commonly derived from laboratory compression tests based on the generalized de-rating factor, which was originally developed from gold mines in the 1980’s (Robert *et al*. 1987). Following these industrial guidelines, no incident has been reported in the past that any of these timbers failed in the London Underground, except the cross-passage incident at Victoria, where the full overburden loading induced by the train vibration was carried (Mackenzie 2014).

Timbers are often used in underground mining. Szwedzicki (1989) argued that the safety factor for timber supports in underground mining was too high, as no sign of stress was observed in many timber packs. Recently, in-situ load measurement has enabled better understanding of the real performance of elongate support units. For example, Daehnke *et al*. (2000) evaluated the performance characteristics of eighteen 140 mm diameter mine poles instrumented with standard pre-stressing units, and six 170 mm diameter mine poles without pre-stressing units spread at four locations of two mines. Direct comparison between the field and laboratory testing results subjected to oblique loading conditions indicated that the relationship proposed by Robert *et al*. (1987) had overestimated the strength of mine poles installed in situ, attributing this overestimation to the effects of installation angle and rotation during the loading process. Piper and Malan (2008) used a wired load logger to measure the in-situ loads on four types of timber elongates with diameters ranging from 160 mm to 180 mm in a shallow platinum mine under very low rates of closure. Their measurements indicated that the original de-rating factor was too conservative; a de-rating factor of up to 40% for low closure areas may be appropriate to take into account of the differences between laboratory and field conditions. Bierman *et al*. (2013) proposed a revised de-rating methodology for timber elongates by recognizing that the original de-rating factor may underestimate their in-situ performance.

These past studies imply that the real performance of timber structures in underground construction could be very site-specific, and can only be understood in conjunction with the environment and real-time ground behavior that they support. The design of timber-based support system should be based on the measurements at that site, and not on the de-rating factors or measurements from others (Piper and Malan 2008). The use of timber for temporary ground support in tunnelling in London Clay has been extensively adopted for over one hundred years, due to the satisfactory physical properties of London Clay. Large components of the face timbering are used to manage the stability of advancing tunnel faces. Cement grout is then pumped into voids between the irregular excavated clay surfaces and the close timbering to avoid soil softening and loss of ground, and to act as a primitive seal by preventing clay to be exposed to the air in the tunnel. These London practices have heavily influenced the traditional timbering in other cohesive soil in the UK (Mackenzie 2014). Unfortunately, based on our best knowledge, there has been no in-situ measurement or evidence made in underground construction to validate its timbering design philosophy.

With the advances in sensor technology, the wireless sensor system has emerged as an alternative to the traditional sensor system. The use of wireless sensor network allows faster deployment, less complication in maintaining the system and better Signal-to-Noise Ratio (SNR) compared to a wired solution. It can facilitate continuous monitoring of critical underground infrastructures with minimum human involvement (Bhalla *et al*. 2005, Hoult *et al*. 2009, Bennnet *et al*. 2010a, b). However there are other challenges such as robust wireless communication to overcome (Akyildiz and Stuntebeck 2006, Stajano *et al*. 2010, Kennedy and Bedford 2014). In this paper, a novel monitoring technology, wireless SmartPlank system, is introduced. Monitoring on a London Underground temporary supporting system is ongoing, using this new technology to understand the actual field behavior of these timber structures.

2. Wireless sensor network

A wireless SmartPlank system measures the field performance of temporary timber structures used in manual underground construction in order (i) to examine the validity engineering assumptions made in design and (ii) to use it as real time monitoring system for safety of construction workers. It consists of an instrumented plank (SmartPlank), some relay sensors and a gateway. The engineering information measured by SmartPlank is transmitted in real-time over an IPv6-based multi-hop wireless mesh network and Internet while the underground construction is taking place. The main advantages of wireless against wired are (i) its ease to be installed in confined space by construction workers due to safety reason and (ii) continuous monitoring of the structures from the installation stage.

2.1 SmartPlank

SmartPlank is a wooden beam equipped with a streamlined wireless sensor node, and two thin foil strain gauges accompanied with two temperature sensors. It measures the strain and temperature experienced by the beam, and transmits this information in real-time through a multi-hop mesh network.

A typical installation of SmartPlank consists of a horizontal head tree supported by two vertical side trees using Yankee brob (see Fig. 1). The top tree takes bending load while the side trees hold the vertical load axially and the lateral bending load. With this layout, strain gauges and temperature sensors are attached on both the top and bottom surfaces of the timber plank. A wireless sensor node is attached to the underside to allow wireless communication. A load cell can be placed at the top of the side tree at the Yankee brob and connected to another wireless sensor node (this was not done in this study). The top tree is countersunk by having the side trees shortened to accommodate the load cells, which enables a constant height for all timber frames.

A 5 mm wire lead strain gauge was used in this study. To avoid the usage of inflammable epoxy adhesives on site, a special mounting plate (60 mm×20 mm×5 mm) using Aluminum alloy 6082 (see Fig. 2(a)) was designed and manufactured. The ends of the plate were made to be thick to ensure a good load transfer from the plank to the gauge. Strain gauges were glued onto the middle thin part of the plate to minimize its local reinforcement effect, and flexible wiring was soldered onto the strain gauge electrical leads. The mounting plate equipped with strain gauge was then mounted to the timber surface on the bottom and top sides to measure both tension and compression during the bending.

A temperature gauge MCP9700A (see Fig. 2(b)) was also attached to the plank surface alongside with each strain gauge to account for any effects that temperature variation might have on the strain gauge. It is a low-cost analog temperature sensor that converts temperature to analog voltage and then digitized by the sensor node. The accuracy of the sensor is ±2˚C for a temperature range from 0˚C to 70˚C, and the operating current is only $6\mu A$.

The electrical wiring from all strain gauge units and temperature gauges is connected to the wireless sensor node attached to the bottom side of the timber plank. The sensor node has 4 input channels, each of which can accept a resistive sensor. Each input channel forms one leg of a Wheatstone bridge and is also connected to ADS7795 Analogue to Digital converter (ADC). ADS7795 is a multi-channel ADC and has an internal amplifier with software selectable gain in powers of 2 from 1 to 128. Each channel can be individually powered and read to keep the total power consumption down to meet the limitations of the battery. The gain of each channel can also be set individually. ADS7795 also has an internal temperature sensor that measures ambient temperature. Each wireless sensor node is powered by either 2 AA size batteries mounted directly on the PCB of the sensor node or by an external pack of 2 D sized Lithium-thionyl Chloride batteries to provide extended operating lifetime. Each sensor node starts sampling the strain gauges and the temperature sensors, and transmits this information through its radio interface. There is a trade-off between the frequency of readings and the battery life. The reading frequency is set in software, and is typically chosen to take a set of readings every 15 minutes for the first week, and then take hourly readings afterwards. It is expected that the nodes will remain in place and will not be recoverable.

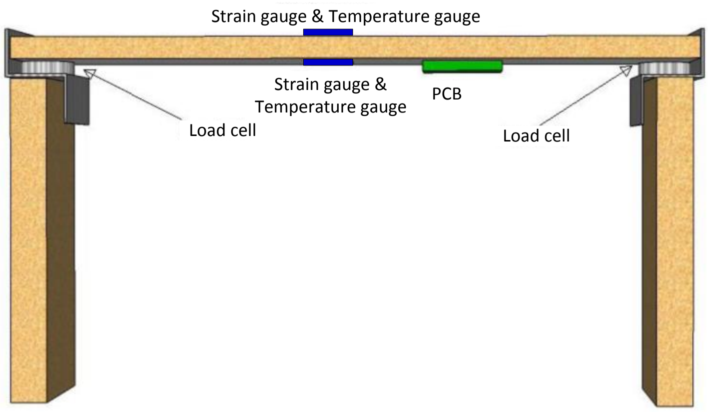

Fig. 1 Idealized SmartPlank prototype

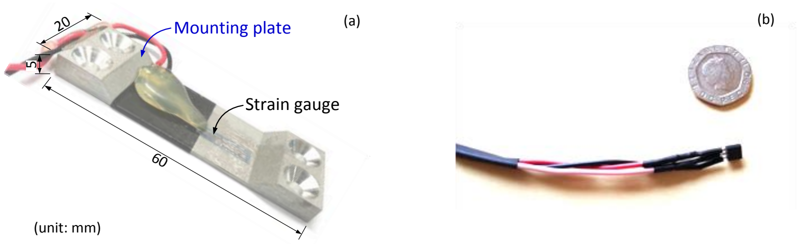

Fig. 2 Sensors mounted on the SmartPlank: (a) strain gauge mounting plate and (b) temperature gauge

2.2 Wireless network

Each wireless sensor node is programmed with application software that has been developed in Contiki OS, an open source operating system for embedded and resource constrained devices. This application software periodically switches on individual channels, powers up the ADS7795, writes configuration commands to it to set input channel and amplifier gain and then samples 10 measurements from each channel. It computes the mean and median values of these measurements and then transmits this information over the wireless network. The input channel and ADS7795 are then powered down. Each sensor nodes uses the IPv6 (6LowPan) stack provided by Contiki OS to form a multi-hop network with nearby SmartPlank nodes and relay nodes.

A relay node is identical to a SmartPlank sensor node except that it does not include any strain gauge or temperature sensors. Its role is to provide connectivity between SmartPlank sensor nodes and the gateway. The 6LowPan network layer includes neighbor discovery, address configuration and packet routing capabilities. It discovers neighboring nodes and maintains the shortest route to the gateway based on link layer packet loss to neighboring nodes. When a data packet destined for the gateway is passed down to the network layer, it looks up the next hop node in its routing table and transmits it to this neighbor. At each node this process continues until the data packet is delivered to the gateway.

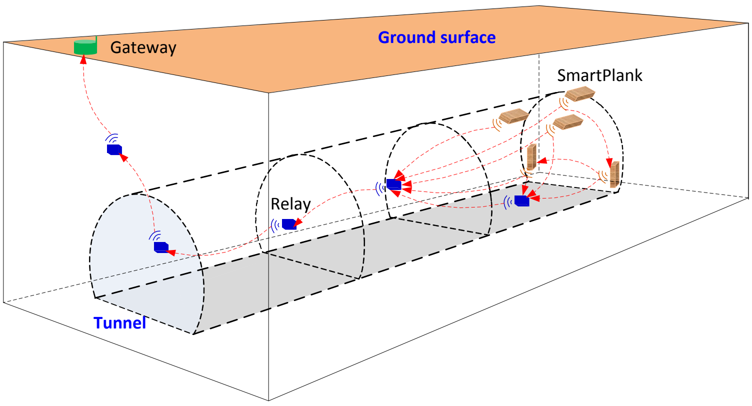

Fig. 3 Wireless sensor network in underground tunnel

The gateway provides local data storage and connectivity to the Internet via a 3G modem. The IPv6 based network allows each sensor node to send data to any host machine over the Internet. It also becomes a host to connect to individual sensor nodes as well. Each node also implements radio duty cycling in software, and switches its radio on with a frequency of 8Hz to sample the radio channel. If it senses any radio transmission, it keeps the radio on to receive the entire packet, otherwise the radio is switched off to save energy.

The received sensor data from strain gauges and temperature sensors is first converted into voltage, and then into strain and temperature measurements. The strain is obtained by using gauge resistance (e.g., 120 Ω for RS strain gauge), and gauge factor (GF) which is a fundamental parameter of the strain gauge defined as the ratio of fractional change in electrical resistance to the fractional change in length. The typical GF for foil strain gauges is around 2.1. The measurement from the temperature sensor can be translated by using the temperature coefficient (10mV/℃ for MCP9700A) and the output voltage at zero degrees (500mV for MCP9700A). Note that temperature compensation is essential to obtain the real strain.

It is vital that the whole system is connected together and tested prior to the real deployment. This is not only to check the network connectivity, but also to assess the capability of each SmartPlank (e.g., strain gauge attachment). To replace the installed problematic planks on real site would become rather difficult, as most of the sites will be inaccessible and unreachable during the excavation period. Calibration of SmartPlank was also conducted in the laboratory to understand the relationship between the actual desired measurements and the collected signal data. Loading tests were conducted with strain gauges directly attached to the wooden beam and with the strain gauge holders next to the directly attached gauges. Results show that the system measures the strain of the instrumented beam accurately.

3. SmartPlank deployment at TCR

London Underground's Tottenham Court Road (TCR) station is currently being upgraded to meet the expected rise in passenger numbers interchanging between London Underground services and Crossrail in 2018. One sub-project is to provide a new access from Stair 14 to the Central Line platforms to reduce congestion. Temporary works have been installed from the Stair 14 upper landing since August 2013, in order to create space and lifting facilities for the installation of the modular channels and top strut above the platform tunnel shoulder during the Central Line possession in 2015. The reinforced concrete, and steel frames together with timber were employed to support the ground after excavation. The deployment of wireless SmartPlank system was carefully designed to comply with the site conditions and the timber temporary system.

3.1 Geological conditions

The geological sequence at Stair 14 comprises of a thin layer of Made Ground and Thames River Terrace Gravels, underlain by the London Clay formation, Harwich formation, the Lamebth Group formation, the Thanet Sand formation then the Chalk, as shown in Fig. 4. The Central Line platform tunnels are entirely within London Clay. The proposed platform level at the Stair 14 opening is 100.445 m TD (tunnel datum), and the existing platform tunnel axis levels varies between 101.6 mTD and 101.9 mTD. The borehole data shows that the reduced levels of the boundaries between strata are similar with no noticeable dipping or faulting. The pore pressure profile is likely to be severely under-drained at this location as the site lies in the middle of the main cone of depression caused by abstraction from the deep aquifer in central London. Therefore, groundwater levels are expected to be around 65 mTD. Further details of the site can be found in Yeow *et al*. (2014).

3.2 SmartPlank deployment

From the completed Stair 14 upper landing, the temporary works were constructed in sequence from stage I to stage VI, as shown in Fig. 5. At each cross-section, up to 20 frames of heading timber were constructed along the line of the modular channels, resting on the H-shaped steel beam frames which were bolted into the concrete walls. The siding and heading H-shaped steel beams are UC 152×152×37 and UC 203×203×46, respectively. The grade of timber used in the temporary support system was C24, with Young's modulus of 9GPa.

Four SmartPlanks numbered as SP51, SP52, SP53 and SP54 were deployed at TCR Stair 14, as shown in Fig. 5(a), each with a rectangular cross-section of 200 mm×100 mm (see Fig. 5(b)). For each SmartPlank, the designed locations for each support were first marked. A strain gauge and a temperature sensor were then attached in the mid-span of both the top and bottom surfaces of the plank, and the wireless sensor node was attached on the bottom side of the timber, as shown in Fig. 6(a). The electrical wiring that connects all the sensing units and the wireless sensor node was wrapped to the side of the plank. This is to avoid direct damage to the wiring during the H-beam installation. Once prepared, each SmartPlank was tested to check its connectivity, and take the baseline readings prior to being installed. The instrumented SmartPlanks were then wrapped with tape to protect them from any physical damage.

The SmartPlanks were installed together with the other planks once the designated location was ready, and were switched on immediately after the installation. Although the planks were supposed to be supported by four bearings (as shown in Fig. 5(a) for SP54), in reality there were only the first and fourth ones available at the initial stage. Wedges were used to stabilize all the planks, which could induce a certain amount of axial force in the planks. It was witnessed that the soil could actually hold itself without failing before the planks were installed. Grouting was then carried out immediately after the timber heading at each stage, to prevent softening and loss of ground (see Fig. 5(a)). The grout also acts as a primitive seal to prevent the clay being exposed to the air in the tunnel. All the bolt holes on the timber head trees were protected during the grouting. The other two steel bearings in the middle were then added a week or so later after the plank installation. Fig. 6(b) gives a picture of SP52 installed at Stair 14 TCR. It is worth noting that the antenna had to be extended and hung down to provide good wireless communication among each node.

3.3 Wireless sensor network at TCR

The wireless monitoring system was deployed at TCR Stair 14 to monitor the field performance of timber heading, including 4 SmartPlanks, 7 relays and a gateway, as shown the plan view in Fig. 7. The initial plan was to spread the relays along the tunnel and connect the gateway with 3G signal, so the data can be sent back to a server in Cambridge. Unfortunately there was very poor 3G signal coverage in the vicinity of the station. As a result, the gateway was moved to the current position shown in Fig. 7, and formed a wireless network. In the mean time, SP51 was not properly installed at the very beginning, and thus became unrecoverable and useless in the end. Monitoring with the other three SmartPlanks is still ongoing.

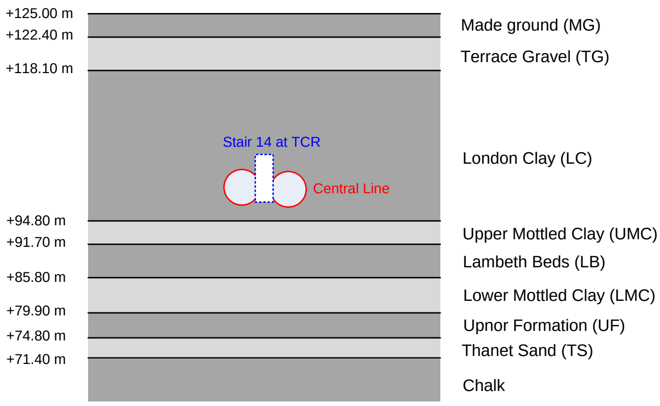

Fig. 4 Geological strata levels at Stair 14, Tottenham Court Road Station, London

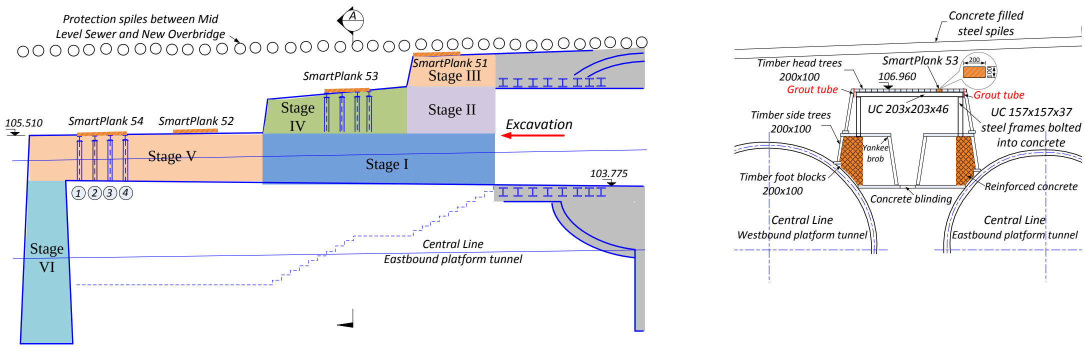

(a) Longitudinal view (b) Sectional view (A-A)

Fig. 5 SmartPlank deployment TCR Stair 14

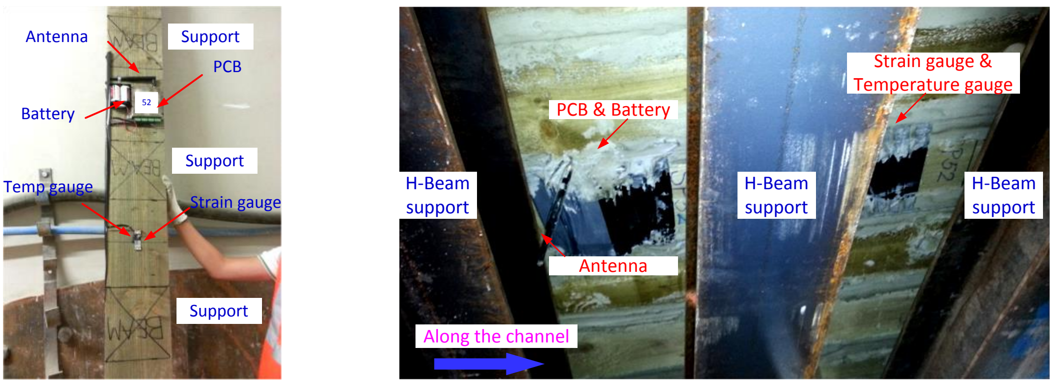

(a) before installation (b) after installation

Fig. 6 Instrumented SmartPlank at TCR Stair 14

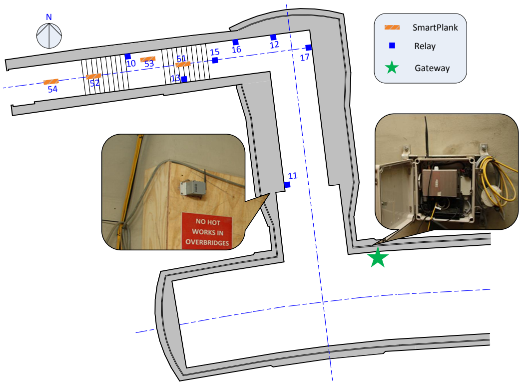

Fig. 7 Wireless sensor network deployment at TCR Stair 14 (plan view)

4. Field performance of SmartPlanks

The SmartPlank monitoring at TCR Stair 14 does indicate movement of the timber supporting system, which will be discussed more in detail here, including observations on both the short-term and long-term performance.

4.1 Cement hydration

Fig. 8 presents the temperature variations captured by the temperature sensors attached on SP52. The first packet of data was received just before the grouting. From Fig. 8, it is observed that the temperature on the top surface of SP52 rose up to 33 degrees around 10 hours after the grouting, and it then gradually decreased to about 25.6 degrees. This is consistent with the classical hydration process of Portland cement. Meanwhile, the temperature variation inside the tunnel is also being monitored by both the temperature sensor in PCB and temperature gauge, with very close measurements. Most of the time, the temperature experienced on the top surface was much higher than the one measured at the bottom, except one occasion on 27th September 2013 probably attributed to the lighting nearby. The maximum and residual temperature differences were up to 10.5 and 2.8 degree respectively.

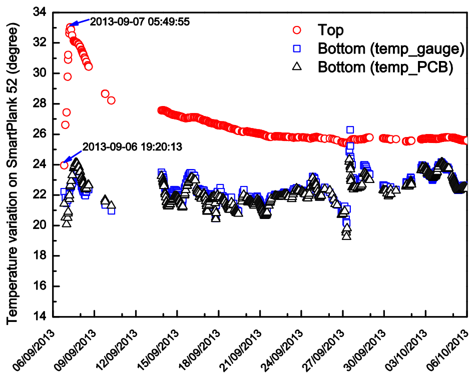

Fig. 8 Temperature variations on SmartPlank 52

4.2 Short-term mechanical performance

Fig. 9(a) illustrates the strain variations experienced on both the top and bottom surfaces of S52 within one month from its installation. The negative strain means compression. It can be clearly observed from Fig. 9(a) that the top surface initially suffered from a very large compression immediately after its installation and then gradually recovered, while the strain happened on the bottom part was much smaller than that of the top part. During the grouting, the peak compression strain was up to 2139.4 micro-strains. This suggests that the grouting had created a downward pressure from the top surface of the plank, together with a pair of extra axial forces, as indicated in Fig. 10. In the meantime, the observed peak compression strain may well exceed the elastic range of the timber, inducing some plastic or permanent damage (Buchanan 1990, Fiorelli and Dias 2003).

The strain on the top surface then dropped rapidly to 41.4% of the peak compression strain when the corresponding temperature reached its maximum value (see Fig. 9). It continued to recover another 24.9% of the maximum compression strain during the cement hardening and shrinking, resulting in a residual compression strain of about 352.8 micro-strains. The SmartPlank was not experiencing pure bending, as there was a residual axial force induced by its installation using wedges. Very similar recovery phenomenon of the compression strain on the top surface of the SmartPlank was also observed from our first pre-trial at Victoria Station (not reported here).

Another instrumented plank, SP54, was the last one installed. At the very beginning of the grouting, the collected strain data on both the top and bottom surfaces indicated that the SmartPlank was largely compressed on both sides, as shown in Fig. 9(b). Unfortunately, a few days after the grouting, it was discovered that there were significant amount of oxidized components in the sensor nodes, caused by unexpected grouting-induced corrosion. The motes stopped working. The oxidized components and the batteries were replaced 24 days after the sensor corrosion due to site inaccessibility. Clearly, extra waterproof precautions must be employed to better protect the sensor nodes. Nevertheless, on the basis of previous analysis, the performance of SP54 was reconstructed, as shown in Fig. 9(b).

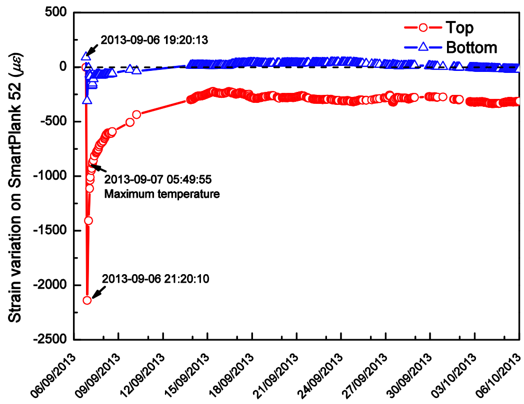

(a) SmartPlank 52

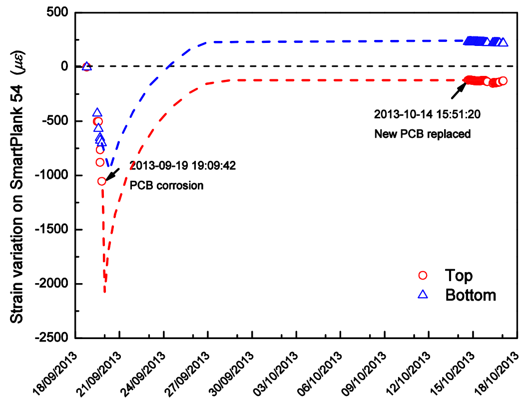

(b) SmartPlank 54

Fig. 9 Short-term performance of SmartPlanks

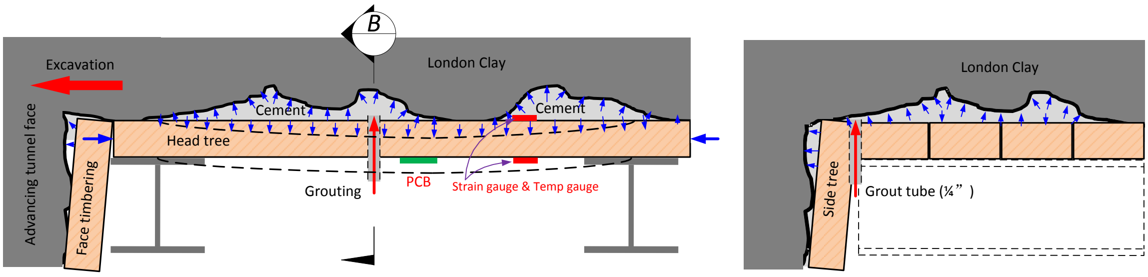

(a) longitudinal view (b) cross-section view (B-B)

Fig. 10 Grouting effect on SmartPlanks

4.3 Long-term mechanical performance

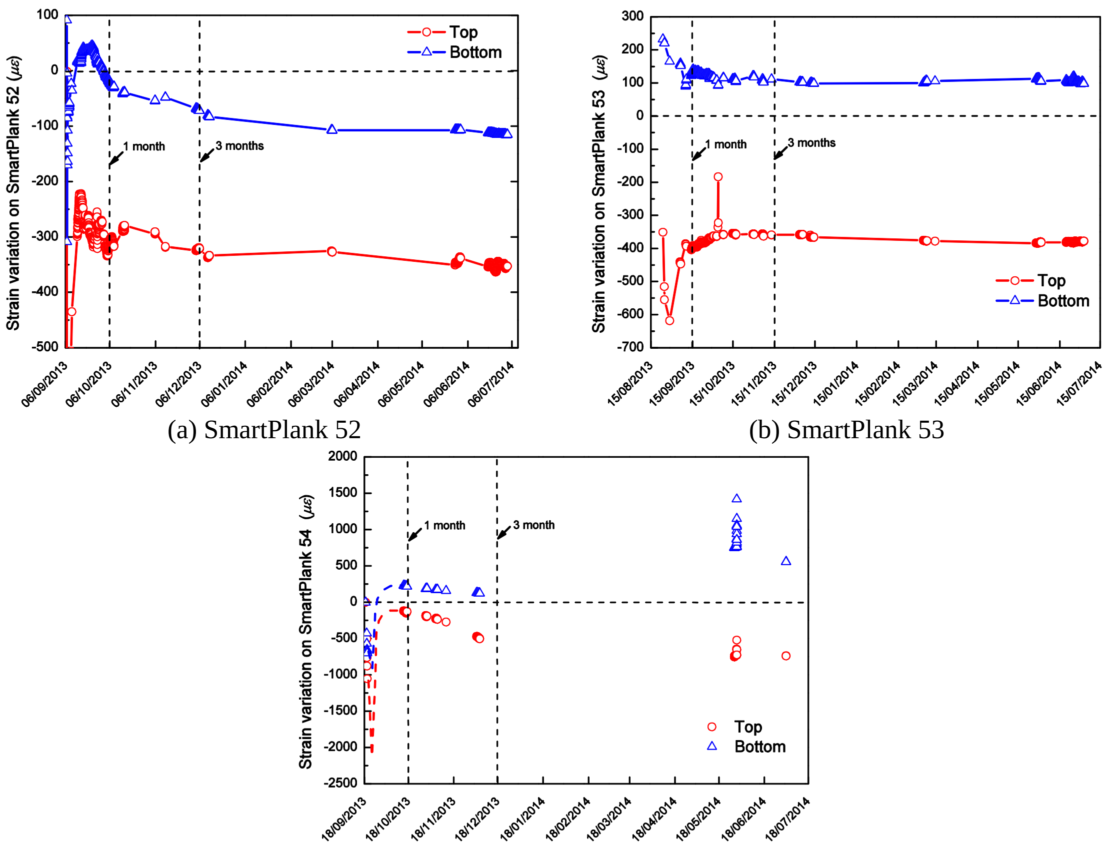

(a) SmartPlank 52 (b) SmartPlank 53

(c) SmartPlank 54

Fig. 11 Long-term performance of timber structures

Fig. 11 presents the long-term performance of SmartPlanks at Stair 14 over a period of 10 months after the installation. It can be observed the figure that all three SmartPlanks continued to deform after the short-term. From December 2013 to May 2014, the data delivery was limited due to antenna damage as well as Contiki software and gateway problems. Despite this, on the basis of the strain rate, their deforming characteristics can be divided into two stages: (1) from 1 month to 3 months; (2) after 3 months. At the first stage, the strain varies in a more rapid way compared to that of the second stage, together with some strain fluctuations. Taking SP52 for an example, the strains on the top and bottom surface vary in a very similar slope, and the average strain rates for both stages are about -0.89 με/day and -0.19 με/day respectively, as shown in Fig. 11(a). For SP53, Fig. 11(b) indicates that there were no clear differences between the strain rates of the two stages mentioned above. Instead, the second stage seems to start from the 1st month, rather than the 3rd one. This is probably due to the relatively high location of SP53, and the protection of the spiles, as shown in Fig. 5.

For SP54, it is obvious from Fig. 11(c) that the strain rates at the 1st stage were much higher than that of the other two. The averaged strain rates for the bottom and top surfaces were up to 1.91 με/day and 7.91 με/day respectively. This attributed to the adjacent deep excavation at stage VI, as shown in Fig. 5(a). At the second stage, although there was not much data collected, some large strain fluctuations were observed at the end of May 2014. Two continuous cracks developed on each side of the walls from November 5th, 2013, between the 2nd and 3rd supports for SP54 (see Fig. 5(a)). The width of the cracks is up to 1mm. This suggests that SP54 experienced some localized movement which may result in the large strain measured.

5. Earth pressure

By assuming a uniformly distributed load, the earth pressure acting on the instrumented planks was estimated using the measured strain according to the beam theory. Two models were adopted to consider different support conditions, and the results are then compared with the current design.

5.1 Simplified model

In this study, a uniformly distributed load is assumed, and two different supporting conditions, namely a simply supported beam (Case 1) and a three-span continuous beam (Case 2), are taken into account, as shown in Fig. 12. All the supports are modeled as elastic bearings, rather than fixed supports, to characterize the contribution from their supporting H-beam frames. The vertical stiffness k_v of the elastic support is obtained by calculating the deformation of the steel frame using the virtual displacement method, and the results are: 42.85 MN/m, 85.69 MN/m and 43.52 MN/m for SP52, SP53 and SP54, respectively. The relatively higher value of stiffness for SP53 is due to its eccentric location, as illustrated in Fig. 7. The horizontal stiffness k_h of the support is simply assumed to be ten times of the vertical ones, but the selection of k_h will not affect the following results in this study.

In Case 1 (see Fig. 12(a)), we assume that each SmartPlank is a simply supported beam during the whole loading process. This implies that the two additional supports placed later (as stated in section 3.2) were not activated at any time. The earth pressure time history $p(t)$ for each SmartPlank is then obtained using the purely bending strain $\varepsilon(t)$. In Case 2 (see Fig. 12(b)), on the other hand, the strain history of each SmartPlank is first divided into two parts: $\varepsilon(t_1)$ for the purely bending strain measured within the first week of installation and $\varepsilon(t_2)$ for additional strain measured from the second week after its installation. Note that their interpretations toward to the earth pressure are performed separately. The first part of earth pressure time history $p(t_1)$ is calculated in the same way as that in Case 1, using $\varepsilon(t_1)$. However, the second part of earth pressure time history $p(t_2)$ depends on the incremental strain $\Delta\varepsilon(t_2)$, which is taken as the difference between $\varepsilon(t_2)$ and the purely bending strain in a week after the installation ε_0. If $\Delta\varepsilon(t_2)$ is negative, $p(t_2)$ is calculated as the superposition of the earth pressure in a week p_0 and the incremental earth pressure $\Delta p(t_2)$. The former is obtained based on the simply supported beam using ε_0, while the latter is calculated based on the three-span continuous beam using $\Delta\varepsilon(t_2)$. Otherwise, $p(t_2)$ is computed in the same way as that in Case 1, using $\varepsilon(t_2)$.

5.2 Earth pressure

Fig. 13 presents the back calculated vertical earth pressure histories on the two of three SmartPlanks based on the abovementioned two cases. For SP52 as shown in Fig. 13(a), the estimated pressure within the grouting period is 100.60kPa. This matches well to the actual grouting pressure measured (approximately 100 kPa). For the post-grouting stage, there was almost no difference between the two cases, except the period between 21st and 26th September 2013, as indicated in the inset of Fig. 13(a). This is probably due to the adjacent construction work (e.g., prop installation) during that period. The residual earth pressure is estimated to be 13.06 kPa, which corresponds to 3.53% of the total overburden vertical stress σ_v.

For SP53, as shown in Fig. 13(b), most of the data was lost during the grouting stage. The estimated residual earth pressure is 26.92kPa (7.87% of σ_v) for Case 1 and 27.13kPa (7.93% of σ_v) for Case 2. For SP54, the estimated pressure is 75.37kPa (20.34% of σ_v) for Case 1 and 594.92kPa (160.57% of σ_v) for Case 2. The result from Case 2 for SP54 seems to be significantly over-estimated, which is possibly due to some localized pressure with two major cracks observed on the siding walls, as discussed earlier. Therefore, for SP54, the assumption of uniformly distributed load may not be appropriate. Further investigation is needed.

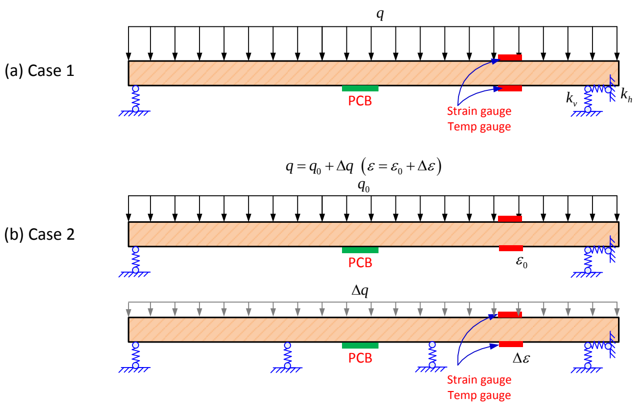

Fig. 12 Longitudinal section of TCR Stair 14

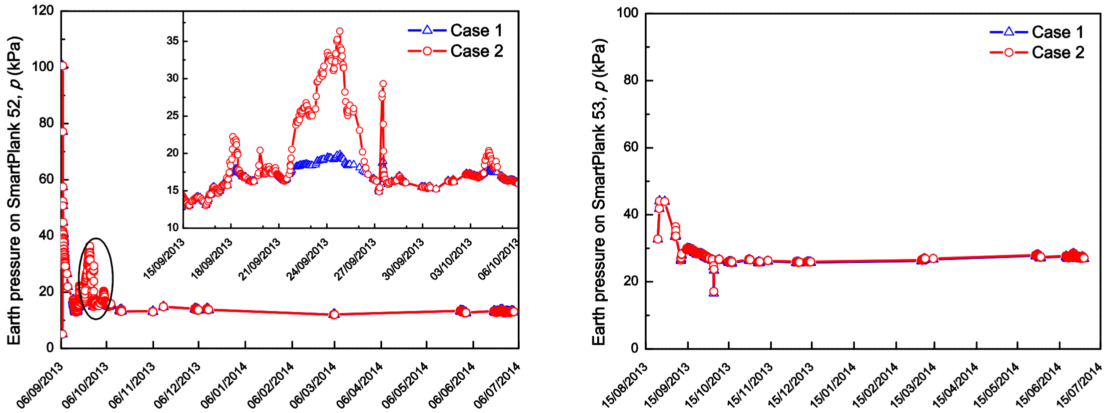

(a) SmartPlank 52 (b) SmartPlank 53

Fig. 13 Calculated earth pressure

5.3 Discussions

Considering the embedded depth, the total vertical overburden pressures σ_v for SP52/SP54 and SP53 are 370.5kPa and 342kPa, respectively. In the design, using Terzarghi's arching theory, the short-term load varies between 15% and 25% of the full overburden for the proposed excavation width at Stair 14. These loads then increase to around 40% of the overburden for the long-term loading condition. The temporary works design comprises of short-term components, timber headings, used to create sufficient space to install the longer-term support elements, steel frames and reinforced concrete. At the design stage, the design load using 25% of the full overburden for short-term ground load was considered to be too conservative, as the installation of stiff concrete filled steel spiles in the Mid-level Sewer in Oxford Street would limit the ground loads acting on the timber headings constructed below (see Fig. 5). Therefore, the design loads for Stair 14 were taken as 15% and 40% respectively, rather than 25% and 40% (Mackenzie 2014).

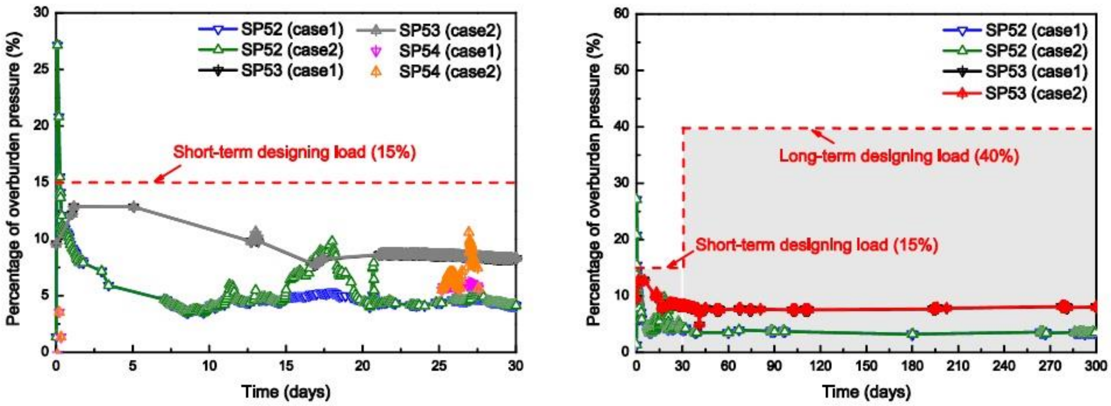

(a) Short-term (b) Long-term

Fig. 14 Comparison between the calculated earth pressure and the designing load

Fig. 14(a) presents a comparison between the estimated earth pressure ratio for the three SmartPlanks and the short-term designing load. As shown in Fig. 14(a), there is not much difference for all three SmartPlanks. The measurements from SP52 rose up to 27.15% during the grouting stage. After that, all the measurements became well below the design load 15%. This indicates that the short term performance of the planks is governed by the grouting process, which is not considered as part of the short-term earth pressure design.

For the long-term earth pressure, as shown in Fig. 14(b), the data recorded so far for the past 10 months indicates that the straining of SP52 and SP53 has stabilized, and hence it is difficult to evaluate whether there are any differences in short and long-term design loads. After 10 months of tunneling, the normalized earth pressures estimated using Case 1 and Case 2 are 3.53% and 3.53% for SP52, and 7.87% and 7.93% for SP53, which appear to be much smaller than the design value of 40%. However, for SP54, the uncertainty in the support made it difficult to evaluate whether the applied earth pressure is within the range of the design value. The effect of localized deformation observed at this location was discussed earlier.

Given the underestimation and overestimation of the short-term and long-term earth pressures on the timber structures respectively, there is an opportunity to improve their design. A set of simple empirical rules for timbering (e.g., an optimized grouting pressure) could largely reduce the timbering components in mass and dimension, and thus reduce the health and safety risks, as well as the construction time and cost. Further investigation is ongoing.

5. Conclusions

This paper proposed a novel wireless sensor network technology to monitor the field performance of timber structures in underground construction. The capability of the system developed was demonstrated through a case study at Stair 14 temporary works, TCR, London. The use of SmartPlank offers an opportunity to improve our understanding on the field performance of the timber structures, which could lead to an optimized design, and a reduced health and safety risk to workers. Ultimately it can be used for real-time monitoring of timber structures to ensure safety of the workers. The key findings are summarized as follows.

- Grouting effect on the short-term performance of timber: the top surface of SP52 experienced a large compression strain during the grouting, and it then gradually recovered even after the hydration rate reaches the peak. The grouting-induced compression strain could be up to 0.22%, which may cause some plastic or permanent damage on the timber. The grouting effect may be minimized by reducing the grouting pressure, or strengthening the support before grouting.
- Cement hydration: the cement hydration process was observed, with temperature rising up to 33 degrees around 10 hours after grouting.
- Timber long-term performance: all three SmartPlanks continued to deform over a period of 10 months after their installation. The deforming process can be divided into two stages: from 1 month to 3 months and after 3 months. For SP52, the strain change at the first stage was around 4.7 times faster than that of the second stage. Much quicker strain change was observed on SP54 probably due the localized deformation caused by nearby construction.
- Earth pressure: results from all three SmartPlanks indicate that the short term performance of the planks was governed by the grouting process, which is not considered as part of the short-term earth pressure design. For the long-term earth pressure, the normalized pressures

estimated from the strain data of SP52 and SP53 were between 3% and 8%, which are much smaller than the design value of 40%. Although the strain development at present is rather small, the planks will be monitored until 2015 to further evaluate their long-term performance.

Acknowledgments

The authors acknowledge the technical assistance from Dr. Jize Yan, Mr. JJ Tang, Dr. Loizos Pelecanos, Mr. Peter Knott, Mr. Samondra Boodhoo and Mr. Alex Alchin. The funding of this project comes from London Underground Limited and the Cambridge Centre for Smart Infrastructure and Construction supported by EPSRC and TSB. The second author acknowledges the support from the Major State Basic Research Development Program of China (973 Program) (No. 2011CB013803).

References

Akyildiz, I.F. and Stuntebeck, E.P. (2006), “Wireless underground sensor networks: research challenges”, *Ad Hoc Networks*, **4**, 669-686.

Bennnet, P.J., Kobayashi, Y., Soga, K. and Wright, P. (2010a), “Wireless sensor network for monitoring of underground tunnel”, *Proceedings of the ICE, Geotechnical Engineering GE3*, **163**, 147-156.

Bennnet, P.J, Soga, K., Wassell, I.J., Fidler, P., Abe, K., Kobayashi, Y. and Vanicek, M. (2010b), “Wireless sensor networks for underground railway applications: case studies in Prague and London”, *Smart Struct. Syst.*, **6**(5-6), 619-639.

Bhalla, S, Yang, Y.W., Zhao, J. and Soh, C.K. (2005), “Structural health monitoring of underground facilities – Technological issues and challenges”, *Tunn. Undergr. Sp. Tech.*, **20**, 487-500.

Bierman, R., Piper, P., Carstens, R. and Priest, G. (2013), “A revised timber elongate de-rating factor for platinum mines”, *Proceedings of the South African National Institute of Rock Engineering Symposium*.

Buchanan, A.H. (1990), “Bending strength of lumber”, *J. Struct. Eng. - ASCE*, **116**(5), 1213-1229.

Daehnke, A., Watson, B.P., Roberts, D., Acheampong, E. and van Zyl, M. (2000), *The impact of soft loading conditions on the performance of elongate support elements*, Safety in Mines Research Advisory Committee, Final Project Report.

Fiorelli, J. and Dias, A.A. (2003), “Analysis of the strength and stiffness of timber beams reinforced with carbon fiber and glass fiber”, *Mater. Rese.*, **6**(2), 193-202.

Hoult, N.A., Bennnet, P.J., Stoianov, I., Maksimović, C., Middleton, C.R., Graham, N.J.G. and Soga, K. (2009), “Wireless sensor networks: creating ‘Smart Infrastructure’”, *Proceedings of ICE, Civil Engineering*, **162**, 136-143.

Kavvadas, M.J. (2003), “Monitoring and modelling ground deformations during tunneling”, *Proceedings of the 11th FIG Symposium on Deformation Measurements*, Santorini, Greece.

Kennedy, G.A. and Bedford, M.D. (2014), “Underground wireless networking: A performance evaluation of communication standards for tunneling and mining”, *Tunn. Undergr. Sp. Tech.*, **43**, 157-170.

Mackenzie ,C.N.P. (2014), “Traditional timbering in soft ground tunneling”, *The British Tunnelling Society*.

Mark, C. and Barczak, T.M. (2000), “Fundamentals of coal mine roof support”, *Proceedings of the New technology for coal mine roof support*, Pittsburgh, USA.

Piper, P.S. and Malan, D.F. (2008), “The in-situ performance of elongate support – myths and realities”, *Proceedings of the 6th International Symposium on Ground Support in Ming and Civil Engineering Construction*, Cape town, South Africa.

Robert, M.K.R., Riemann, K. and Jager, A.J. (1987), *The performance characteristics of timber props*, Chamber of Mines Research Organisation, Research Report.

Stajano, F., Hoult, N.A., Wassell, I.J., Bennett, P.J., Middleton, C.R. and Soga, K. (2010), "Smart bridges, smart tunnels: transforming wireless sensor networks from research prototypes into robust engineering infrastructure", *Ad Hoc Networks*, **8**, 872-888.

Szwedzicki, T. (1989), "Geotechnical assessment deficiencies in underground mining", *Mining Sci. Technol.*, **9**, 23-37.

Terzaghi, K. (1946), *An introduction to tunnel geology*, in Rock Tunnelling with Steel Supports, (Eds., Proctor R.V. and White T.L.), The Commercial Shearing and Stamping Co, Youngstown, Ohio, USA.

Yeow, H.C., Nicholson, D. and Man, C.L. (2014), "Application of observational method at Crossrail Tottenham Court Road station, UK", *Geotech. Eng.*, **167**(2), 182-193.